

Simultaneous Multicolor Photometry of the DESTINY⁺ target asteroid (3200) Phaethon

Jin BENIYAMA^{1,2,*}, Tomohiko SEKIGUCHI³, Daisuke KURODA^{4,5}, Tomoko ARAI⁶, Ko ISHIBASHI⁶, Masateru ISHIGURO^{7,8}, Fumi YOSHIDA^{6,9}, Hiroaki SENSHU⁶, Takafumi OOTSUBO¹⁰, Shigeyuki SAKO^{1,11,12}, Ryou OHSAWA¹⁰, Satoshi TAKITA¹, Jooyeon GEEM^{7,8} and Yoonsoo P. BACH^{7,8}

¹Institute of Astronomy, Graduate School of Science, The University of Tokyo, 2-21-1 Osawa, Mitaka, Tokyo 181-0015, Japan

²Department of Astronomy, Graduate School of Science, The University of Tokyo, 7-3-1 Hongo, Bunkyo-ku, Tokyo 113-0033, Japan

³Asahikawa Campus, Hokkaido University of Education, Hokumon, Asahikawa, Hokkaido 070-8621, Japan

⁴Okayama Observatory, Kyoto University, 3037-5 Honjo, Kamogata-cho, Asakuchi, Okayama 719-0232, Japan

⁵Bisei Spaceguard Center, Japan Spaceguard Association, 1716-3 Okura, Bisei, Ibara, Okayama 714-1411, Japan

⁶Planetary Exploration Research Center, Chiba Institute of Technology, 2-17-1 Tsudanuma, Narashino, Chiba, 275-0016, Japan

⁷Department of Physics and Astronomy, Seoul National University, 1 Gwanak-ro, Gwanak-gu, Seoul 08826, Republic of Korea

⁸SNU Astronomy Research Center, Seoul National University, 1 Gwanak-ro, Gwanak-gu, Seoul 08826, Republic of Korea

⁹School of Medicine, Department of Basic Sciences, University of Occupational and Environmental Health, 1-1 Iseigaoka, Yahata, Kitakyusyu 807-8555, Japan

¹⁰National Astronomical Observatory of Japan, 2-21-1 Osawa, Mitaka, Tokyo 181-8588, Japan

¹¹UTokyo Organization for Planetary Space Science, The University of Tokyo, 7-3-1 Hongo, Bunkyo-ku, Tokyo 113-0033, Japan

¹²Collaborative Research Organization for Space Science and Technology, The University of Tokyo, 7-3-1 Hongo, Bunkyo-ku, Tokyo 113-0033, Japan

*E-mail: beniyama@ioa.s.u-tokyo.ac.jp

Received 2022 December 16; Accepted

Abstract

Accurate estimation of brightness of (3200) Phaethon up to lower phase angles are essential for planning of the on-board camera of the DESTINY⁺ mission. We have carried out intensive observations of Phaethon in the optical wavelength (g , r , and i) with the TriCCS camera on the Seimei 3.8 m telescope in October and November, 2021. We derived the absolute magnitude H_V and the slope parameter G of Phaethon as $H_V = 14.23 \pm 0.02$ and $G = 0.040 \pm 0.008$ from multiple photometric observations including lower phase angles down to $\sim 9^\circ$ with the H - G model. Using the H_V value and the geometric albedo of Phaethon derived in previous polarimetric studies, we estimated that the Phaethon's diameter is within a range of 5.22 to 6.74 km, which is consistent with radar and occultation observations. With the linear model, we derived

$H_V = 14.65 \pm 0.02$, which corresponds to a diameter range of 4.30 to 5.56 km. Our simultaneous tricolor lightcurves of Phaethon indicate that no rotational spectral variations larger than 0.018 and 0.020 mag in the g-r and r-i colors, possibly related to inhomogeneity of the surface material and/or structure, are seen at the 2021 apparition.

Key words: methods: observational — techniques: photometric — minor planets, asteroids: individual (Phaethon)

1 Introduction

The asteroid (3200) Phaethon is one of the most attractive asteroids: dust activity near the perihelion (Jewitt & Li 2010; Jewitt et al. 2013; Li & Jewitt 2013; Hui & Li 2017), near-Sun and near-Earth orbits (Ohtsuka et al. 2009), and the parent body of the Geminid meteor shower (Williams & Wu 1993). Phaethon was discovered in images of the Infrared Astronomy Satellite (IRAS) in 1983 (Green & Kowal 1983). Phaethon approaches Sun every about 1.4 years with a large eccentricity, ~ 0.89 , and an extremely small perihelion distance, ~ 0.14 au. The perihelion activities were reported in 2009, 2012, and 2016 by observations with the Solar TERrestrial RELations Observatory (STEREO) spacecraft (Jewitt & Li 2010; Jewitt et al. 2013; Li & Jewitt 2013; Hui & Li 2017). Phaethon is taxonomically classified as B-type in the Bus taxonomy (Bus 1999; Bus & Binzel 2002).

Phaethon is selected as a target of the exploration mission Demonstration and Experiment of Space Technology for INterplanetary voYage Phaethon fLyby and dUst Science, DESTINY⁺ (Arai et al. 2018). The DESTINY⁺ is a mission proposed for the JAXA/ISAS Epsilon class small program and will be launched in 2024 (Arai et al. 2018; Arai et al. 2022; Ozaki et al. 2022). Since the rendezvous is difficult for Phaethon with a large relative velocity arise from the large eccentricity and orbital inclination, the DESTINY⁺ will flyby Phaethon in 2028 (Arai et al. 2018). High-resolution imaging with the panchromatic telescopic camera (TCAP) and the VIS-NIR multi-band camera (MCAP) will be performed at the flyby. To succeed just one DESTINY⁺ flyby with Phaethon, we need to know its surface brightness with high accuracy beforehand. It is desired that the on-board camera setting, such as sensor gain and exposure time, are fixed before the flyby since the time is limited to change the camera setting just before the approach due to the large relative velocity at the flyby.

The disk-integrated brightness dependence on the solar phase angle is called a phase curve. The phase curve provides an estimate of an absolute magnitude H , the apparent magnitude of an object located 1 au apart from Sun

and Earth at zero phase angle. In general, we inevitably derive the H by extrapolating the phase curve because it is difficult to obtain photometric data at the zero phase angle. For Phaethon, Ansdell et al. (2014) reported the absolute magnitude in the Johnson R -band, H_R , as 13.90 in observations at phase angles of 12 to 83°. Tabeshian et al. (2019) derived the H_R as 13.28 ± 0.02 in observations at phase angles of 20 to 100°. The derived absolute magnitudes have a discrepancy. In addition, there may be a systematic uncertainty in the absolute magnitude of Phaethon since no observation at phase angles α below 12° has been reported. That is to say, the disk-integrated brightness for Phaethon is still unclear, especially at lower phase angles. To derive the absolute magnitude with high accuracy, additional observations at lower phase angles are necessary. An investigation of the surface inhomogeneity of Phaethon is also one of the most important tasks to do before the DESTINY⁺ flyby. Several surface features on Phaethon such as concavities and boulders have been reported by radar observations (Taylor et al. 2019). To know the local terrain of Phaethon's surface by ground-based observations before the flyby is important for the DESTINY⁺ mission because they can adjust the flyby timing to observe the interesting side of Phaethon.

Rotational color variations can reflect the surface inhomogeneity of asteroids. In previous studies, color variations of Phaethon were detected by spectroscopic (Licandro et al. 2007; Kareta et al. 2018; Lazzarin et al. 2019; Ohtsuka et al. 2020) and multicolor photometric observations (Tabeshian et al. 2019; Lin et al. 2020). Recently, MacLennan et al. (2022) found an evidence of the heterogeneity of surface grain size on Phaethon among different latitudes with thermophysical modeling (TPM) using the latest shape model constructed with radar data as well as optical lightcurves. However, uniform colors of Phaethon in longitude are also reported (Borisov et al. 2018; Lee et al. 2019). The inhomogeneity of Phaethon's surface is still debated and follow-up observations in other apparitions are required.

The aims of this study are to constrain H_V and G parameters and to investigate Phaethon's surface inhomogeneity before the DESTINY⁺ flyby. We carried out si-

multaneous multicolor photometry of Phaethon in 2021. Simultaneous multicolor observations allow us to achieve accurate measurements of the surface colors since the simultaneity cancels out the atmospheric variations in the measurements. In this paper, we will describe observations and data reduction in section 2. The results are compared with previous studies in section 3. In section 4, we discuss the absolute magnitude, diameter, and inhomogeneity of Phaethon.

2 Observations and data reduction

2.1 Observations

We conducted multicolor photometry with the TriColor CMOS Camera and Spectrograph (TriCCS) on the Seimei 3.8 m telescope (Kurita et al. 2020) in Okayama, Japan. The observing conditions are summarized in table 1. We obtained g , r , and i -band images with the Pan-STARRS filters simultaneously with TriCCS. The field of view of each $2k \times 1k$ CMOS image sensor is $12'.6 \times 7'.5$ with a pixel scale of 0.350 arcsec.

Phaethon was observed on nine nights in October and November, 2021. On the first day, October 27th, we set the exposure time as 30 s and realized that the signal-to-noise ratio was not enough to discuss the surface inhomogeneity. Then, we set nominal exposure times as 60 s from October 28th to achieve a high signal-to-noise ratio.

The telescope was operated in the non-sidereal tracking mode to follow Phaethon during our observations with ephemerides from NASA JPL/HORIZONS¹. Elongations of the point spread functions (PSF) of stars in the images (hereinafter referred to as reference stars) were negligible since Phaethon's angular velocities in the observations were small enough compared to a typical PSF, 2–5 arcsec in full width at half maximum (FWHM). The observation fields were crowded with reference stars since Phaethon was located close to the galactic plane at the time of our observations (galactic latitude $|b| < 20^\circ$, figure 1).

2.2 Data reduction

2.2.1 Photometry

After standard corrections (bias subtraction, dark subtraction, and flat-field correction), cosmic ray events were removed using the Python package `astroscrappy` (McCully et al. 2018) based on Pieter van Dokkum's `L.A.Cosmic` algorithm (van Dokkum 2001). The standard circular aperture photometry was done on Phaethon and reference stars in each frame using the SExtractor-based Python package

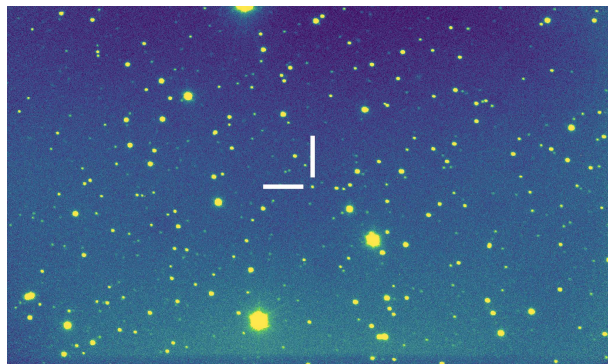


Fig. 1. Image of (3200) Phaethon in r -band with a 60 s exposure in October 28th, 2021 taken by TriCCS. Field of view covers $12'.6 \times 7'.5$. North is to the top and East is to the left.

`sep` (Bertin & Arnouts 1996; Barbary et al. 2015). The aperture radius was set to 2 times larger than the FWHM of the PSF of reference stars. The FWHM of the PSF in each frame was calculated using reference stars before the photometry. The light-travel time correction was done to obtain the time-series colors and magnitudes (Harris & Lupishko 1989).

Stars meet any criterion below were not used in the analysis: uncertainties in g , r , or i -band magnitudes in Pan-STARRS Data Release 2 (DR2, Chambers et al. 2016) are larger than 0.05 mag, $(g-r)_{\text{PS}} > 1.1$, $(g-r)_{\text{PS}} < 0.0$, $(r-i)_{\text{PS}} > 0.8$, or $(r-i)_{\text{PS}} < 0.0$, where $(g-r)_{\text{PS}}$ and $(r-i)_{\text{PS}}$ are colors in Pan-STARRS system. Also, we removed photometric results close to the edges of the image (200 pixels from the edge) or with any other sources in its aperture frame by frame. Extended sources, possible quasars, and variable stars were removed using the `objinflag` and `objfilterflag` in Pan-STARRS DR2.

2.2.2 Color and magnitude derivation

Simultaneous multicolor observations are a reliable method to measure the accurate colors of asteroids. We derived the Phaethon's surface colors in the slightly different manner in Jackson et al. (2021)². We used the linear relationship between instrumental colors and colors in the Pan-STARRS system as follows:

$$(g-r)_{\text{PS},m}^n = \text{CTG}_{g-r}(g-r)_{\text{inst},m}^n + \text{CTI}_{g-r}^n, \quad (1)$$

$$(r-i)_{\text{PS},m}^n = \text{CTG}_{r-i}(r-i)_{\text{inst},m}^n + \text{CTI}_{r-i}^n, \quad (2)$$

where m is the index of the object, n is the index of the frame, $(g-r)_{\text{inst},m}^n$ and $(r-i)_{\text{inst},m}^n$ are instrumental colors of m -th object on the n -th frame, CTG_{g-r} and CTG_{r-i} are color transformation gradients (CTGs) of the $g-r$ and

² The differences are filter bands and airmass dependences of first items in equations (3)–(5). While our first items, instrumental magnitudes, depend on airmass, theirs do not.

¹ <https://ssd.jpl.nasa.gov/?horizons>

Table 1. Summary of the observations.*

Obs. Date (UTC)	T_{exp} (s)	N_{img}	V (mag)	Velocity (arcsec h ⁻¹)	α (°)	Δ (au)	r_{h} (au)	Airmass	Note
2021-10-27 14:03:30–20:14:54	30	585	17.9	46.6	15.9	1.4602	2.3133	1.01–1.28	
2021-10-28 11:56:47–20:08:57	60	408	17.9	47.4	15.6	1.4498	2.3107	1.01–1.87	photometric
2021-10-29 13:29:30–20:19:49	60	318	17.8	49.2	15.2	1.4380	2.3075	1.01–1.34	
2021-11-10 10:34:33–20:27:50	60	304	17.5	64.8	10.3	1.3286	2.2683	1.00–1.89	photometric
2021-11-11 10:27:49–20:13:04	60	357	17.4	66.0	10.0	1.3215	2.2647	1.00–1.87	
2021-11-12 10:19:30–20:25:47	60	435	17.4	67.2	9.7	1.3148	2.2611	1.00–2.01	photometric
2021-11-24 12:40:26–18:56:40	60	186	17.2	79.1	9.1	1.2614	2.2126	1.00–1.99	
2021-11-25 09:30:53–17:15:42	60	267	17.2	78.7	9.3	1.2597	2.2088	1.00–1.60	photometric
2021-11-26 09:31:57–18:48:41	60	408	17.2	79.1	9.6	1.2580	2.2044	1.00–2.06	photometric

* Observation time in UTC (Obs. Date), exposure time (T_{exp}), and the number of images (N_{img}) for each night are listed. Predicted V -band apparent magnitude (V), angular rate of change in apparent RA and DEC (Velocity), phase angle (α), distance between Phaethon and observer (Δ), and distance between Phaethon and Sun (r_{h}) at the observation starting time are from NASA JPL/HORIZONS as of 2022-11-8 (UTC). Elevations to calculate air mass range (Airmass) are also from NASA JPL/HORIZONS.

$g-r$ colors, respectively, and CTI_{g-r}^n and CTI_{r-i}^n are color transformation intercepts (CTIs) of the $g-r$ and $r-i$ colors on the n -th frame, respectively. First, we derived the CTGs at the night by the linear fitting of the photometric results of the reference stars during the night. To determine the unique CTGs at the night, the photometric results were shifted frame by frame to cancel out the atmospheric variations in CTIs. After the derivation of CTGs, the CTIs in each frame were calculated with the derived CTGs with equations (1) and (2). Phaethon's colors were derived from the instrumental colors, fixed CTGs, and CTIs. We computed the propagated uncertainties of $(g-r)_{\text{PS}}$ and $(r-i)_{\text{PS}}$ with the photometric errors and uncertainties of the CTGs and CTIs.

The same as color derivations, we used the linear relationship to derive the magnitudes as follows:

$$g_m^n = g_{\text{inst},m}^n + \text{CT}_g(g-r)_{\text{PS},m}^n + Z_g^n, \quad (3)$$

$$r_m^n = r_{\text{inst},m}^n + \text{CT}_r(g-r)_{\text{PS},m}^n + Z_r^n, \quad (4)$$

$$i_m^n = i_{\text{inst},m}^n + \text{CT}_i(g-r)_{\text{PS},m}^n + Z_i^n, \quad (5)$$

where g_m^n , r_m^n , and i_m^n are magnitudes in the Pan-STARRS system of m -th object on the n -th frame, $g_{\text{inst},m}^n$, $r_{\text{inst},m}^n$, and $i_{\text{inst},m}^n$ are instrumental magnitudes of m -th object on the n -th frame, CT_g , CT_r , and CT_i , are color terms (CTs) of g , r , and i -band magnitudes, respectively, and Z_g^n , Z_r^n , and Z_i^n are zero points of g , r , and i -band magnitudes on the n -th frame, respectively. The same as colors, we firstly derived CTs at the night while shifting the photometric results of the reference stars during the night frame by frame so that the atmospheric variations in instrumental magnitudes and Z s were canceled out. Then, the Z s in each frame were calculated with the derived CTs with equations (3)–(5). We computed the propagated uncertainties of g , r , and i -band magnitudes with the photometric errors and uncertainties of $(g-r)_{\text{PS}}$, CTs and Z s.

2.2.3 Periodic analysis

We used the Lomb-Scargle method for periodic analysis (Lomb 1976; Scargle 1982; VanderPlas 2018). The detail of the periodic analysis is summarized in Beniyama et al. (2022). The purpose of the periodic analysis in this study is not to derive the rotation period of Phaethon, but to create fitting curves to estimate the mean magnitude, which is essential for the phase curve fitting. Thus, we referred to the reported rotation period of Phaethon $P = 3.603957 \pm 0.000001$ h (Kim et al. 2018; Hanuš et al. 2018) and fixed it to determine the Fourier coefficients of the model curve. Since the Phaethon's sidereal and synodic periods during our observations have little difference (~ 1.2 s, Harris et al. 1984), we referred to the Phaethon's sidereal period derived in the previous studies.

2.2.4 Phase curve fitting

The reduced g , r and i -band magnitudes, g_{red} , r_{red} , and i_{red} , were obtained by scaling the distances from both Earth and Sun to Phaethon to 1 au as follows:

$$g_{\text{red}} = g - 5 \log_{10} \Delta r_{\text{h}}, \quad (6)$$

$$r_{\text{red}} = r - 5 \log_{10} \Delta r_{\text{h}}, \quad (7)$$

$$i_{\text{red}} = i - 5 \log_{10} \Delta r_{\text{h}}, \quad (8)$$

where Δ and r_{h} are geocentric and heliocentric distances in the unit of au at the time of observation. With the same Fourier coefficients of the model curve created in section 2.2.3 except for the constant term (i.e., mean magnitude), we searched the optimal constant term to minimize the residuals between the model and the observations. The averages of the reduced magnitudes $g_{\text{red,mean}}$, $r_{\text{red,mean}}$, and $i_{\text{red,mean}}$, were derived as constant terms of the Fourier series of the shifted model curve (see dotted lines in figure 7 in the Appendix 1).

The $g_{\text{red,mean}}$ and $r_{\text{red,mean}}$ were converted to R -band

magnitudes using the equation in Tonry et al. (2012) to refer to Ansdell et al. (2014) for data at other phase angles, in which Phaethon was observed with *R*-band filter (see section 3.4 for detail). In section 3.4, we used two types of models in phase curve fitting to derive the absolute magnitude and the slope parameter.

The posterior distributions of the parameters were estimated using the Monte Carlo technique. We created 1000 phase curves by randomly sampling the observed data points assuming that every point follows a normal distribution. We adopted the standard deviations as the uncertainties of the parameters. The median (50th percentile) and 95 % highest density interval (HDI) values were obtained.

3 Results

3.1 The comet-like activity

The comet-like activity near the perihelion, possibly related to the dust production, was reported for Phaethon (Jewitt & Li 2010; Jewitt et al. 2013; Li & Jewitt 2013; Hui & Li 2017). Though Phaethon was far from its perihelion at the time of our observing runs, we searched the comet-like activity of Phaethon in the *r*-band image in October 28th, 2021. A comparison of the radial profile of Phaethon with that of a standard star SA23-433 (Landolt 2013) is shown in figure 2. The standard star SA23-433 was observed in the sidereal tracking mode before the Phaethon's image. The exposure starting times of the images of Phaethon and SA23-433 are 2021-10-28 16:06:55 and 2021-10-28 16:11:38 (UT), respectively. Both images were obtained in similar low-airmass conditions (~ 1.02). The fluxes were averaged in the azimuthal direction from the centroids of Phaethon and SA23-433. The uncertainties of the fluxes consist of the background noise and the Poisson noise in each annulus. Moffat functions were used to fit both radial profiles to derive the FWHMs of the PSFs. The derived FWHMs were 2.46 arcsec and 2.50 arcsec for Phaethon and SA23-433, respectively. The similarity of the radial profile of Phaethon and SA23-433 implies that no noticeable comet-like activity was found in the 2021 apparition.

3.2 Lightcurves

The folded lightcurves with $P = 3.603957$ h (Kim et al. 2018; Hanuš et al. 2018) in nine nights are shown in figure 3.

The fitting model curves (i.e., Fourier coefficients) were obtained using the *g*-band lightcurves on November 24, 25, and 26, adopting the number of harmonics $n = 4$. Each

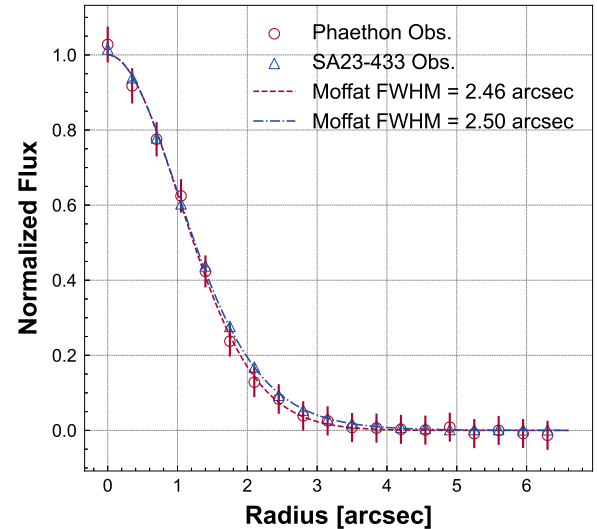


Fig. 2. Radial profiles of Phaethon (circles) and SA23-433 (triangles) in the *r*-band images in October 28th, 2021. The profiles were normalized to the peaks of the Moffat fits (dashed and dot-dashed lines). Bars indicate the $1\text{-}\sigma$ uncertainties.

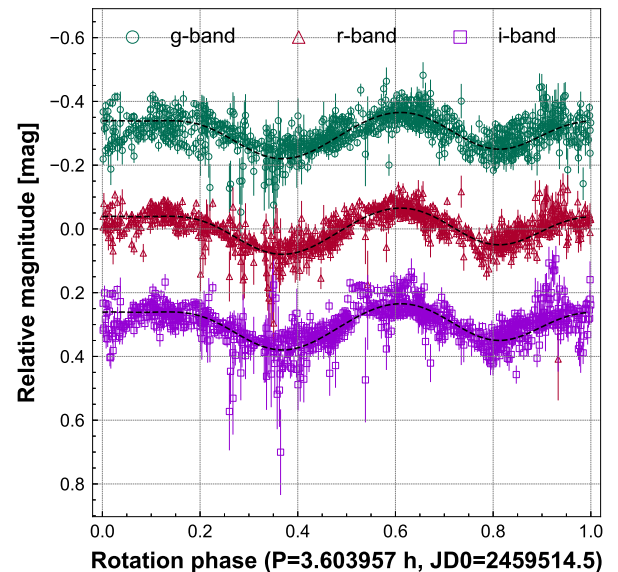


Fig. 3. Phased relative lightcurves of Phaethon in nine nights. From top to bottom, *g* (circles), *r* (triangles), and *i*-band (squares) relative lightcurves in each day are presented. Lightcurves are folded by the reported period of 3.603957 h and phase zero is set to 2459514.5 JD. Bars indicate the $1\text{-}\sigma$ uncertainties. Fitting model curves are shown by dashed lines. Phased lightcurves of Phaethon in each day are attached in figure 7, see the Appendix 1.

lightcurve was shifted to minimize the residuals between the model and the observations considering the constant term (i.e., mean magnitude) as a free parameter. We defined a peak-to-trough variation as a lightcurve amplitude Δm . Assuming the asteroid is a triaxial ellipsoid with axial lengths of a , b , and c ($a > b > c$) and rotating along the c -axis with an aspect angle of 90° , a lower limit of axial ratio a/b is estimated as follows:

$$\frac{a}{b} \geq 10^{0.4\Delta m(\alpha)/(1+s\alpha)}, \quad (9)$$

where $\Delta m(\alpha)$ is a lightcurve amplitude at a phase angle of α and s is a slope depending on the taxonomic type of the asteroid (Bowell et al. 1989). We assumed $s = 0.015$, a typical value for C-type asteroids (Zappala et al. 1990). The lightcurve amplitude of the fitting model curve in the g -band was derived as 0.15 mag, which corresponds to $a/b \geq 1.13$ at $\alpha = 9.1^\circ$.

3.3 Surface colors

The colors in five photometric nights, October 28, November 10, 12, 25, and 26, are shown in figure 4. We calculated the weighted averages of the colors in each night. Here we presume that the systematic uncertainty of colors derived by our observations is 0.02 mag based on the photometry of reference stars (see the Appendix 2). The systematic uncertainties dominate over the statistical uncertainties in derived colors. Then, the weighted average of colors were $g - r = 0.35 \pm 0.02$ and $r - i = 0.08 \pm 0.02$. The color corresponds to $V - R = 0.36 \pm 0.02$ in the Johnson system (Tonry et al. 2012).

We summarized the derived surface colors with those reported in previous studies in table 2. To compare the colors obtained in different filter systems, the color transformations between the Pan-STARRS and the Johnson systems were performed with the equations in Tonry et al. (2012). Since Dundon (2005) in 2004, Jewitt (2013), and Ansdell et al. (2014) did not observe Phaethon in the I -band, we derived only the $g - r$ color in the Pan-STARRS system for them.

3.4 Phase curve

We successfully observed Phaethon at lower phase angles down to about 9° . The phase curves of Phaethon are shown in figure 5. As in subsection 3.3, we limited the results obtained in the five photometric nights.

We combined our observational results with those reported in Ansdell et al. (2014), not Tabeshian et al. (2019). This is because we regard the average of the $B - V$ color in Tabeshian et al. (2019) are different from the colors re-

ported in other studies (table 2). The data set in Ansdell et al. (2014) obtained in November, 2004 and December, 2013 are not used in this paper since those lightcurves are relative rather than absolute without absolute calibrations due to the lack of field stars. We note that observational results in 2013 Nov 13 in Ansdell et al. (2014) are also removed by eye and not used for phase curve fittings since the average of the reduced R -band magnitude is far from other observations.

The uncertainties of $g_{\text{red,mean}}$ and $r_{\text{red,mean}}$ are given as the standard error of the weighted average of the lightcurves. These uncertainties are much smaller than those of the mean R -band magnitudes of our observations (~ 0.015) due to the uncertainties in the magnitude transformation between the Pan-STARRS and the Johnson systems. This is the same for the observation results in Ansdell et al. (2014), but the propagated uncertainties of the mean R -band magnitudes are smaller than ours since there is no magnitude transformation. Taking into account the fact that the lightcurve amplitudes of Phaethon are about 0.1–0.2 mag and not all lightcurves in Ansdell et al. (2014) fully covered the rotation phase, we set the uncertainties of the mean reduced R -band magnitudes in Ansdell et al. (2014) to 0.05 mag. We obtained the mean R -band magnitudes as $R = 14.88 \pm 0.02$ mag at $\alpha = 15.5^\circ$, $R = 14.66 \pm 0.02$ mag at $\alpha = 10.2^\circ$, $R = 14.63 \pm 0.02$ mag at $\alpha = 9.6^\circ$, $R = 14.56 \pm 0.02$ mag at $\alpha = 9.4^\circ$, and $R = 14.55 \pm 0.02$ mag at $\alpha = 9.7^\circ$, where α were the mean solar phase angles at the nights.

First, we derived an absolute magnitude in R -band H_R and a slope parameter G with the H - G model (Bowell et al. 1989):

$$H_R(\alpha) = H_R - 2.5 \log_{10}((1 - G)\Phi_1(\alpha) + G\Phi_2(\alpha)), \quad (10)$$

where α is a phase angle. Φ_1 and Φ_2 are phase functions written as follows with a basic function W :

$$\Phi_1(\alpha) = W \left(1 - \frac{0.986 \sin \alpha}{0.119 + 1.341 \sin \alpha - 0.754 \sin^2 \alpha} \right) + (1 - W) \exp \left(-3.332 \tan^{0.631} \frac{\alpha}{2} \right), \quad (11)$$

$$\Phi_2(\alpha) = W \left(1 - \frac{0.238 \sin \alpha}{0.119 + 1.341 \sin \alpha - 0.754 \sin^2 \alpha} \right) + (1 - W) \exp \left(-1.862 \tan^{1.218} \frac{\alpha}{2} \right), \quad (12)$$

$$W = \exp \left(-90.56 \tan^2 \frac{\alpha}{2} \right). \quad (13)$$

We derived $H_R = 13.87 \pm 0.01$ and $G = 0.040 \pm 0.008$ from model fitting with H - G model in panel (a) of figure 5. H_R were converted to $H_V = 14.23 \pm 0.02$ using the $V - R$ color derived in subsection 3.3. The phase reddening effect is ignored in this study since the colors of B-type asteroids in Bus or Bus-DeMeo taxonomy (DeMeo et al. 2009) are

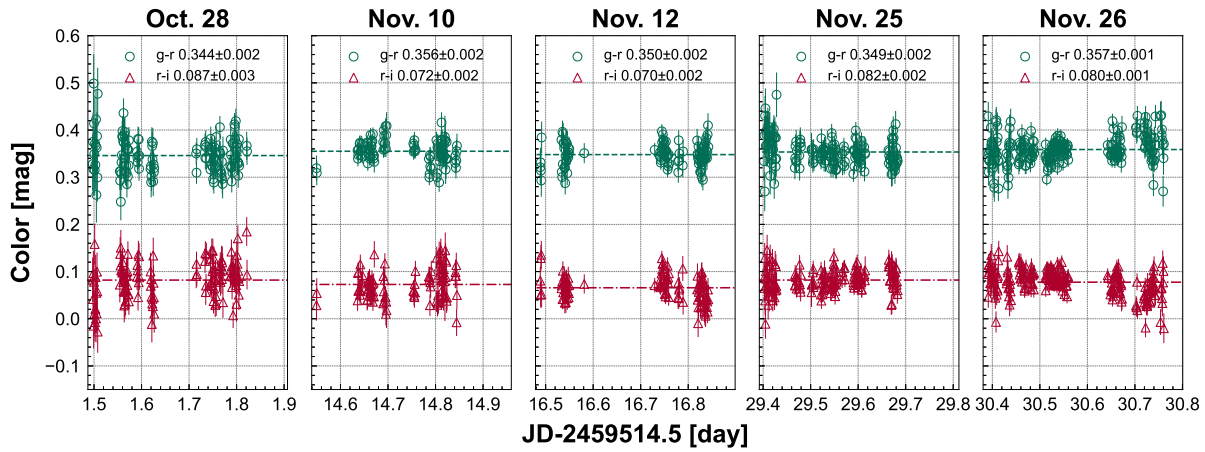


Fig. 4. Colors of Phaethon in five photometric nights. $g-r$ and $r-i$ colors are shown by circles and triangles, respectively. Weighted averages of $g-r$ and $r-i$ colors in each night are presented with dashed and dash-dotted horizontal lines, respectively. Bars indicate the $1-\sigma$ uncertainties.

Table 2. Comparison of Phaethon's surface colors.*

References	Obs. Date (UTC)	$g-r$ (mag)	$r-i$ (mag)	$B-V$ (mag)	$V-R$ (mag)	$R-I$ (mag)
Dundon (2005)	1996 Nov 12	0.37 ± 0.03	—	0.618 ± 0.005	0.347 ± 0.004	—
Dundon (2005)	1997 Nov 22	0.40 ± 0.03	0.08 ± 0.03	0.650 ± 0.004	0.295 ± 0.002	0.320 ± 0.003
Dundon (2005)	2004 Nov 19	0.34 ± 0.03	—	0.587 ± 0.005	0.349 ± 0.003	—
Kasuga & Jewitt (2008)	2007 Sep 04	0.36 ± 0.03	0.03 ± 0.05	0.61 ± 0.01	0.34 ± 0.03	0.27 ± 0.04
Jewitt (2013)	2010 Sep 10	0.42 ± 0.03	—	0.67 ± 0.02	0.32 ± 0.02	—
Ansdell et al. (2014)	1997 Nov 12	0.34 ± 0.03	—	0.58 ± 0.01	0.34 ± 0.02	—
Ansdell et al. (2014)	1997 Nov 22	0.33 ± 0.03	—	0.57 ± 0.01	0.36 ± 0.01	—
Ansdell et al. (2014)	1995 Jan 04	0.28 ± 0.03	—	0.52 ± 0.01	0.33 ± 0.01	—
Lee et al. (2019)	2017 Nov 11–13	0.39 ± 0.03	0.07 ± 0.04	0.64 ± 0.02	0.34 ± 0.02	0.31 ± 0.03
Tabeshian et al. (2019)	2017 Dec 11–19	0.45 ± 0.03	0.03 ± 0.03	0.702 ± 0.004	0.309 ± 0.003	0.266 ± 0.004
Lin et al. (2020)	2017 Oct/Nov/Dec	0.38 ± 0.04	0.10 ± 0.03	0.633 ± 0.036	0.336 ± 0.011	0.334 ± 0.015
Sergeyev & Carry (2021) [†]	2009 Jan 26	0.32 ± 0.03	0.07 ± 0.03	0.56 ± 0.05	0.34 ± 0.03	0.30 ± 0.04
This work	2021 Oct 28	0.34 ± 0.02	0.09 ± 0.02	0.59 ± 0.04	0.35 ± 0.02	0.32 ± 0.03
This work	2021 Nov 10	0.36 ± 0.02	0.07 ± 0.02	0.60 ± 0.04	0.36 ± 0.02	0.31 ± 0.03
This work	2021 Nov 12	0.35 ± 0.02	0.07 ± 0.02	0.60 ± 0.04	0.36 ± 0.02	0.31 ± 0.03
This work	2021 Nov 25	0.35 ± 0.02	0.08 ± 0.02	0.60 ± 0.04	0.36 ± 0.02	0.32 ± 0.03
This work	2021 Nov 26	0.36 ± 0.02	0.08 ± 0.02	0.60 ± 0.04	0.36 ± 0.02	0.32 ± 0.03

* $g-r$, $r-i$ (Pan-STARRS), $B-V$, $V-R$, and $R-I$ (Johnson) colors are listed with their references. Colors derived without any transformation are shown in bold character. Colors derived after transformations based on Tonry et al. (2012) are presented in normal character.

[†] The Pan-STARRS and Johnson colors are converted from the SDSS colors.

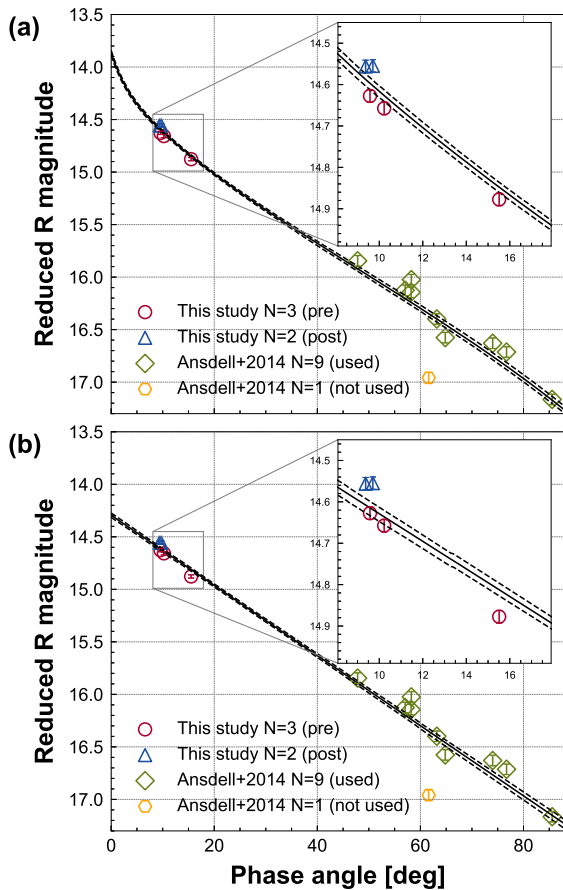


Fig. 5. Phase curves of Phaethon with (a) the H - G and (b) the linear models. Mean reduced R -band magnitudes in 2021 pre-opposition, 2021 post-opposition, and Ansdell et al. (2014) are presented as circles, triangles, and diamonds, respectively. Removed data in Ansdell et al. (2014) are presented as Hexagons (see text for detail). Bars indicate the $1\text{-}\sigma$ uncertainties. Median (50th percentile) of fitting model curves are presented by solid lines. Uncertainty envelopes representing the 95 % HDI values are shown by dashed lines.

known to be almost constant at the phase angle $\alpha \leq 70^\circ$ (Lantz et al. 2018).

Second, we used the linear model:

$$H_R(\alpha) = H_{R,\text{lin}} + a_{\text{lin}}\alpha, \quad (14)$$

where, $H_{R,\text{lin}}$ is an absolute magnitude in the linear model and a_{lin} is a slope of the fitting curve. In panel (b) of figure 5, we derived $a_{\text{lin}} = 0.0334 \pm 0.0003$ and $H_{R,\text{lin}} = 14.29 \pm 0.01$ with the linear model, which corresponds to $H_V = 14.65 \pm 0.02$.

We also tried the phase curve fitting with Shevchenko’s model (Shevchenko 1996), but the fitting curve showed a strong opposition surge. This is possibly due to the lack of observations at lower phase angles ($\alpha \leq 9^\circ$). Thus, we did not derive the absolute magnitude with the Shevchenko model.

4 Discussion

4.1 Updated absolute magnitude

The opposition surge is seen in phase curves with the H - G model in panel (a) of figure 5. This is not the case for the linear model by definition in panel (b) of figure 5. Whether the opposition surge exists in Phaethon’s phase curve is unclear even with our latest results ($\alpha \geq 9^\circ$). Devogèle et al. (2020) found that the phase curve of 2005 UD, which may have the same parent body as Phaethon (Ohtsuka et al. 2006; Jewitt & Hsieh 2006), shows very little or no opposition surge. Although, Phaethon and 2005 UD may have similar properties by chance (Ryabova et al. 2019; Kareta et al. 2021). In that case, the opposition surge may exist in Phaethon’s phase curve. We conservatively derived a possible absolute magnitude range as $H_V = 14.18\text{--}14.66$ with H_R , $H_{R,\text{lin}}$, and their uncertainties considering both cases with and without the opposition surge. The comparison with the phase curve by in-situ observations of DESTINY+ is awaited to investigate the existence of the opposition surge.

4.2 Diameter

We combined our H_V with the latest geometric albedo $p_V = 0.08\text{--}0.13$ derived from polarimetric observations (Geem et al. 2022) to estimate the rotation averaged area-equivalent diameter of Phaethon. The reasons to refer to Geem et al. (2022) are that the albedos can be derived directly from the polarimetric parameters using an empirical equation and they carefully considered all possible uncertainties of constants in the empirical equation. The diameter of an asteroid is estimated with H_V and p_V using the following equation (Fowler & Chillemi 1992):

$$D = \frac{1329}{\sqrt{p_V}} \times 10^{-H_V/5} \text{ km}. \quad (15)$$

The Phaethon’s diameter was estimated to be within the range of $5.22 \leq D \leq 6.74$ km with the H - G model and $4.30 \leq D \leq 5.56$ km with the linear model.

In table 3, we compared the derived Phaethon’s diameter with those estimated by other techniques: radar observations, TPMs, and occultation observations. Taylor et al. (2019) reported the volume-equivalent diameters as 6.2 km and 5.5 km using the Doppler-only echo spectra with the spherical and top-shaped assumptions, respectively. Also, the mean equatorial diameter was derived as 6.25 km using the Range-Doppler technique. Hanuš et al. (2016, 2018) derived a convex shape model of Phaethon and estimated the volume-equivalent diameter as 5.1 ± 0.2 km by the TPM with thermal infrared data taken by IRAS, UKIRT (Green et al. 1985), and Spitzer Space

Telescope in a combination with optical lightcurves. They assumed $H_V = 14.31$ and $G = 0.15$ in their TPM. Masiero et al. (2019) estimated the volume-equivalent diameter as $4.6_{-0.3}^{+0.2}$ km with the spherical assumption by the TPM with thermal infrared data taken by WISE. They assumed $H_V = 14.31 \pm 0.03$ in their TPM. Recently, MacLennan et al. (2022) derived a volume-equivalent diameter of 5.4 ± 0.1 km using a TPM which incorporates AKARI observations (Usui et al. 2011) in addition to the data used in all the prior studies with an accurate non-convex shape model. As for occultation observations, Devogèle et al. (2020) combined Phaethon's convex shape model in Hanuš et al. (2018) and occultation chords in the USA on July 29, 2019. The volume-equivalent diameter is derived as 5.2 ± 0.1 km. Yoshida et al. (2022) reported that the projected size of Phaethon is 6.12 ± 0.07 km \times 4.14 ± 0.07 km by stellar occultation observations in Japan on October 13, 2021. An area-equivalent diameter of a projected ellipse is estimated to be 5.03 ± 0.07 km.

The diameter derived with the H - G model in this study falls into the larger range of diameters. This is consistent with radar and occultation observations. On the other hand, the diameter derived with the linear model falls into the smaller range of diameters, which is consistent with those derived by the TPMs.

4.3 Surface inhomogeneity

We conducted simultaneous tricolor observations of Phaethon for the first time. The simultaneity in the multicolor photometry is crucial to investigate the surface inhomogeneity of the asteroid since it can reduce the effects of atmospheric variations on the measurements.

We referred to two published observational studies on surface spectroscopic variations of Phaethon. By multicolor photometry, Tabeshian et al. (2019) reported a B - V color variation of about 0.1 mag with observations from December 11 to 19 in 2017. They interpreted that the color variation with sub-observer latitude may be associated with craters on the surface since they observed both southern and northern parts in the 2017 apparition. Lin et al. (2020) detected a R - I color variation of 0.037 mag in rotation phase with observations from October 6 to December 21 in 2017. They interpreted that the color variation may be caused by the inhomogeneous surface.

We divided the phased colors into five sections equally and calculated the weighted mean colors as shown in figure 6. The largest deviation from the global mean values are 0.018 mag and 0.020 mag in the $g-r$ and $r-i$ colors, respectively, considering the uncertainties. Color variations in the 2021 apparition are smaller than those reported in

previous studies.

Phaethon's latitudinal surface inhomogeneity can probably explain this inconsistency. As is often the case in near-Earth asteroids, the aspect angles are different in each apparition and sometimes even in the same apparition. We mainly observed the slightly northern part of Phaethon in our observing runs; sub-observer latitudes were calculated with the pole orientation $\lambda = 316^\circ$ and $\beta = -48.7^\circ$ (MacLennan et al. 2022) as 29.7 to 29.2° between Oct. 27 and 29, 25.6 to 24.8° between Nov. 10 and 12, and 19.5 to 18.5° between Nov. 24 and 26. On the other hand, the aspect angle was changed a lot in the 2017 apparition. Thus, our observational result suggests that Phaethon's northern hemisphere is almost homogeneous compared with the southern/northern latitudinal difference seen in Tabeshian et al. (2019). This may be relevant to the latitudinal heterogeneity of the surface grain sizes on Phaethon (MacLennan et al. 2022).

Both the latitudinal surface inhomogeneity and our homogeneous color are not necessarily inconsistent with the color variation in the rotation phase reported in Lin et al. (2020). If the colors in the former (0.0–0.5) and the latter (0.5–1.0) rotation phases in Lin et al. (2020) were derived using the data obtained in the different periods (i.e., aspect angles), this is consistent with the latitudinal surface inhomogeneity. Since there is no detailed information for observations in Lin et al. (2020), such as the observation date and time of each data, further discussion is beyond the scope of this paper. We note that there is a possibility that the reported surface color variation is affected by observational artifacts. The situation is the same for 2005 UD. Kinoshita et al. (2007) detected the surface color variation on 2005 UD by multicolor photometry in 2005. However, Devogèle et al. (2020) did not detect any color variations on 2005 UD by spectroscopy on two nights in 2018. For reliable detections of surface color variation, independent observations (e.g., optical and NIR, López-Oquendo et al. 2022) and/or observations in multiple rotation phases are desired in addition to careful data reduction. As for Phaethon, the DESTINY⁺ mission might put an end to the discussion related to the surface inhomogeneity on Phaethon.

5 Conclusions

We conducted simultaneous tricolor photometry for the first time for the DESTINY⁺ mission target asteroid (3200) Phaethon. By observations at the lower phase angles down to $\sim 9^\circ$, we updated an absolute magnitude H_V and a slope parameter G as $H_V = 14.23 \pm 0.02$ and $G = 0.040 \pm 0.008$ with the H - G model. Assuming geo-

Table 3. Comparison of Phaethon’s Diameters.

References	Methods	Shape	D (km)
Taylor et al. (2019)	Doppler-only	sphere	6.2*
Taylor et al. (2019)	Doppler-only	top-shape	5.5*
Taylor et al. (2019)	Range-Doppler	-	6.25 [†]
Hanuš et al. (2016, 2018)	TPM	convex shape	5.1 ± 0.2*
Masiero et al. (2019)	TPM	sphere	4.6 ^{+0.2*} _{-0.3}
MacLennan et al. (2022)	TPM	non-convex shape	5.4 ± 0.1*
Devogèle et al. (2020)	Occultation	convex shape	5.2 ± 0.1*
Yoshida et al. (2022)	Occultation	ellipse	5.03 ± 0.07 [‡]
This study H - G model + Geem et al. (2022)	Photometry & Polarimetry	-	5.22–6.74 [§]
This study linear model + Geem et al. (2022)	Photometry & Polarimetry	-	4.30–5.56 [§]

* Volume-equivalent diameter

† Mean equatorial diameter

‡ Area-equivalent diameter of a projected ellipse

§ Rotation averaged area-equivalent diameter

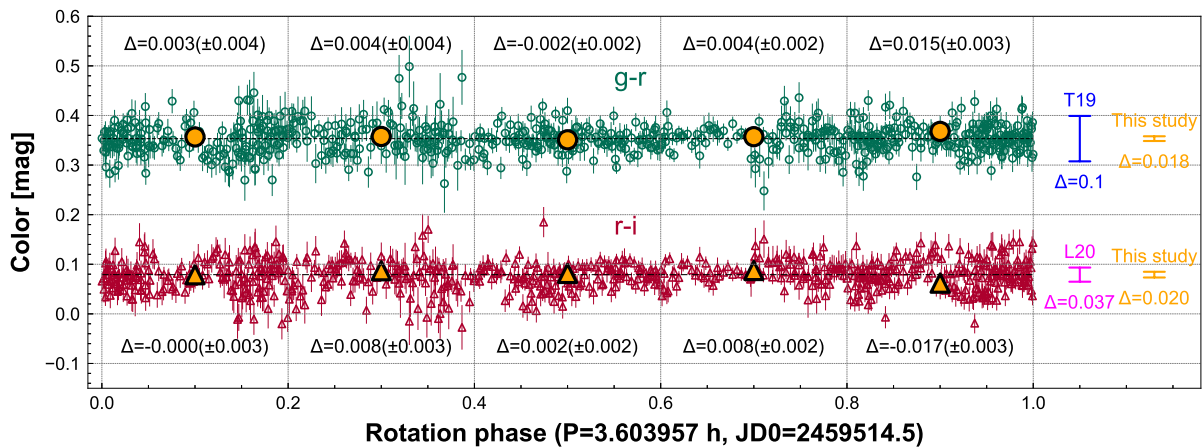


Fig. 6. Phased colors of Phaethon in five photometric nights. $g-r$ and $r-i$ colors are shown by open circles and open triangles, respectively. Weighted average $g-r$ and $r-i$ colors in each night are presented with dashed and dash-dotted horizontal lines, respectively. Weighted average $g-r$ and $r-i$ colors per 0.2 phase are shown by filled circles and filled triangles with derivations from the global average colors. Values in the parentheses are uncertainties of the binned colors. Range corresponding to the color variations reported in Tabeshian et al. (2019, T19), Lin et al. (2020, L20), and this study are presented by arrows on the right.

metric albedo derived by polarimetry, Phaethon’s diameter was estimated to be in the range of 5.22–6.74 km, which is consistent with diameters derived from other techniques such as radar and occultation observations. We derived $H_V = 14.65 \pm 0.02$ with the linear model, which corresponds to a diameter range of 4.30–5.56 km. The diameters by thermophysical modelings should be updated using our derived H_V and G . No noticeable rotational spectral variation was found in our simultaneous multi-color lightcurves in 2021. Our observational result suggests Phaethon’s northern hemisphere is more homogeneous than the southern/northern latitudinal difference reported in previous studies.

Acknowledgments

The authors are grateful to our reviewer Eric MacLennan for helpful comments on the first version of this manuscript. J. B. would like to express my gratitude to the Iwadare Scholarship Foundation and the Public Trust Iwai Hisao Memorial Tokyo Scholarship Fund for the grants. This work is supported in part by the Optical and Near-Infrared Astronomy Inter-University Cooperation Program (OISTER), the Ministry of Education, Culture, Sports, Science and Technology (MEXT) of Japan, JST SPRING, Grant Number JPMJSP2108, and the UTEC UTokyo Scholarship. The authors thank the TriCCS developer team (which has been supported by the JSPS KAKENHI grant Nos. JP18H05223, JP20H00174, and JP20H04736, and by NAOJ Joint Development Research).

Appendix 1 Phased lightcurves

Phased lightcurves in each day are presented here in figure 7.

Appendix 2 Photometric conditions

The photometric results of the reference stars and CTIs are presented in the figures 8 and 9. The color deviations between those in the Pan-STARRS DR2 and those derived here are at most 0.02 mag for the reference stars on October 28, November 10, 12, 25, and 26. Thus, we presume the systematic uncertainty of the colors is 0.02 mag in both $g - r$ and $r - i$. We consider October 28, November 10, 12, 25, and 26 as photometric nights since CTIs are stable on those days.

References

- Ansdell, M., Meech, K. J., Hainaut, O., Buie, M. W., Kaluna, H., Bauer, J., & Dundon, L. 2014, *ApJ*, 793, 50
- Arai, T., et al. 2018, in 49th Annual Lunar and Planetary Science Conference Lunar and Planetary Science Conference. , 2570
- Arai, T., et al. 2022, in 53th Annual Lunar and Planetary Science Conference Lunar and Planetary Science Conference. , 2916
- Barbary, K., Boone, K., & Deil, C., 2015, sep: v1.3.0
- Beniyama, J., et al. 2022, *PASJ*, 74, 877
- Bertin, E., & Arnouts, S. 1996, *A&AS*, 117, 393
- Borisov, G., et al. 2018, *MNRAS*, 480, L131
- Bowell, E., Hapke, B., Domingue, D., Lumme, K., Peltoniemi, J., & Harris, A. W. 1989, in R. P., Binzel, et al., , *Asteroids II*. Tucson, AZ: Univ. Arizona Press
- Bus, S. J., & Binzel, R. P. 2002, *Icarus*, 158, 146
- Bus, S. J. 1999, PhD thesis, Massachusetts Institute of Technology
- Chambers, K. C., et al. 2016, arXiv:1612.05560
- DeMeo, F. E., Binzel, R. P., Slivan, S. M., & Bus, S. J. 2009, *Icarus*, 202, 160
- Devogèle, M., et al. 2020, *PSJ*, 1, 15
- Dundon, L. R. 2005, Master's thesis, University of Hawaii at Manoa, Honolulu
- Fowler, J. W., & Chillemi, J. R. 1992, *Phillips Lab. Tech. Rep.*, 2049, 17
- Geem, J., et al. 2022, *MNRAS*, 516, L53
- Green, S., & Kowal, C. 1983, *IAU Circ.*, 3878, 1
- Green, S. F., Meadows, A. J., & Davies, J. K. 1985, *MNRAS*, 214, 29P
- Hanuš, J., et al. 2016, *A&A*, 592, A34
- Hanuš, J., et al. 2018, *A&A*, 620, L8
- Harris, A. W., & Lupishko, D. F. 1989, in *Asteroids II*, ed. R. P., Binzel, et al. , 39
- Harris, A. W., Young, J. W., Scaltriti, F., & Zappala, V. 1984, *Icarus*, 57, 251
- Hui, M.-T., & Li, J. 2017, *AJ*, 153, 23
- Jackson, S. L., Kolb, U. C., & Green, S. F. 2021, *PASP*, 133, 075003
- Jewitt, D. 2013, *AJ*, 145, 133
- Jewitt, D., & Hsieh, H. 2006, *AJ*, 132, 1624
- Jewitt, D., & Li, J. 2010, *AJ*, 140, 1519
- Jewitt, D., Li, J., & Agarwal, J. 2013, *ApJL*, 771, L36
- Kareta, T., Reddy, V., Hergenrother, C., Lauretta, D. S., Arai, T., Takir, D., Sanchez, J., & Hanuš, J. 2018, *AJ*, 156, 287
- Kareta, T., Reddy, V., Pearson, N., Sanchez, J. A., & Harris, W. M. 2021, *PSJ*, 2, 190
- Kasuga, T., & Jewitt, D. 2008, *AJ*, 136, 881
- Kim, M. J., et al. 2018, *A&A*, 619, A123
- Kinoshita, D., et al. 2007, *A&A*, 466, 1153
- Kurita, M., et al. 2020, *PASJ*, 72, 48
- Landolt, A. U. 2013, *AJ*, 146, 131
- Lantz, C., Binzel, R. P., & DeMeo, F. E. 2018, *Icarus*, 302, 10
- Lazzarin, M., Petropoulou, V., Bertini, I., La Forgia, F., Ochner, P., Migliorini, A., & Siviero, A. 2019, *Planet. Space Sci.*, 165, 115
- Lee, H. J., et al. 2019, *Planet. Space Sci.*, 165, 296
- Li, J., & Jewitt, D. 2013, *AJ*, 145, 154
- Licandro, J., Campins, H., Mothé-Diniz, T., Pinilla-Alonso, N., & de León, J. 2007, *A&A*, 461, 751
- Lin, Z.-Y., et al. 2020, *Planet. Space Sci.*, 194, 105114
- Lomb, N. R. 1976, *Ap&SS*, 39, 447
- López-Oquendo, A., et al. 2022, *PSJ*, 3, 189
- MacLennan, E., Marshall, S., & Granvik, M. 2022, *Icarus*, 388, 115226
- Masiero, J. R., Wright, E. L., & Mainzer, A. K. 2019, *AJ*, 158, 97
- McCully, C., et al., 2018, *Astropy/Astrocrappy: V1.0.5 Zenodo Release*, Zenodo
- Ohtsuka, K., Sekiguchi, T., Kinoshita, D., Watanabe, J. I., Ito, T., Arakida, H., & Kasuga, T. 2006, *A&A*, 450, L25
- Ohtsuka, K., et al. 2020, *Planet. Space Sci.*, 191, 104940
- Ohtsuka, K., Nakato, A., Nakamura, T., Kinoshita, D., Ito, T., Yoshikawa, M., & Hasegawa, S. 2009, *PASJ*, 61, 1375
- Ozaki, N., et al. 2022, *Acta Astronautica*, 196, 42
- Ryabova, G. O., Avdyushev, V. A., & Williams, I. P. 2019, *MNRAS*, 485, 3378
- Scargle, J. D. 1982, *ApJ*, 263, 835
- Sergeyev, A. V., & Carry, B. 2021, *A&A*, 652, A59
- Shevchenko, V. G. 1996, in *Lunar and Planetary Science Conference.* , 1193
- Tabeshian, M., Wiegert, P., Ye, Q., Hui, M.-T., Gao, X., & Tan, H. 2019, *AJ*, 158, 30
- Taylor, P. A., et al. 2019, *Planet. Space Sci.*, 167, 1
- Tonry, J. L., et al. 2012, *ApJ*, 750, 99
- Usui, F., et al. 2011, *PASJ*, 63, 1117
- van Dokkum, P. G. 2001, *PASP*, 113, 1420
- VanderPlas, J. T. 2018, *ApJS*, 236, 16
- Williams, I. P., & Wu, Z. 1993, *MNRAS*, 262, 231
- Yoshida, F., et al. 2022, *PASJ*, in press
- Zappala, V., Cellino, A., Barucci, A. M., Fulchignoni, M., & Lupishko, D. F. 1990, *A&A*, 231, 548

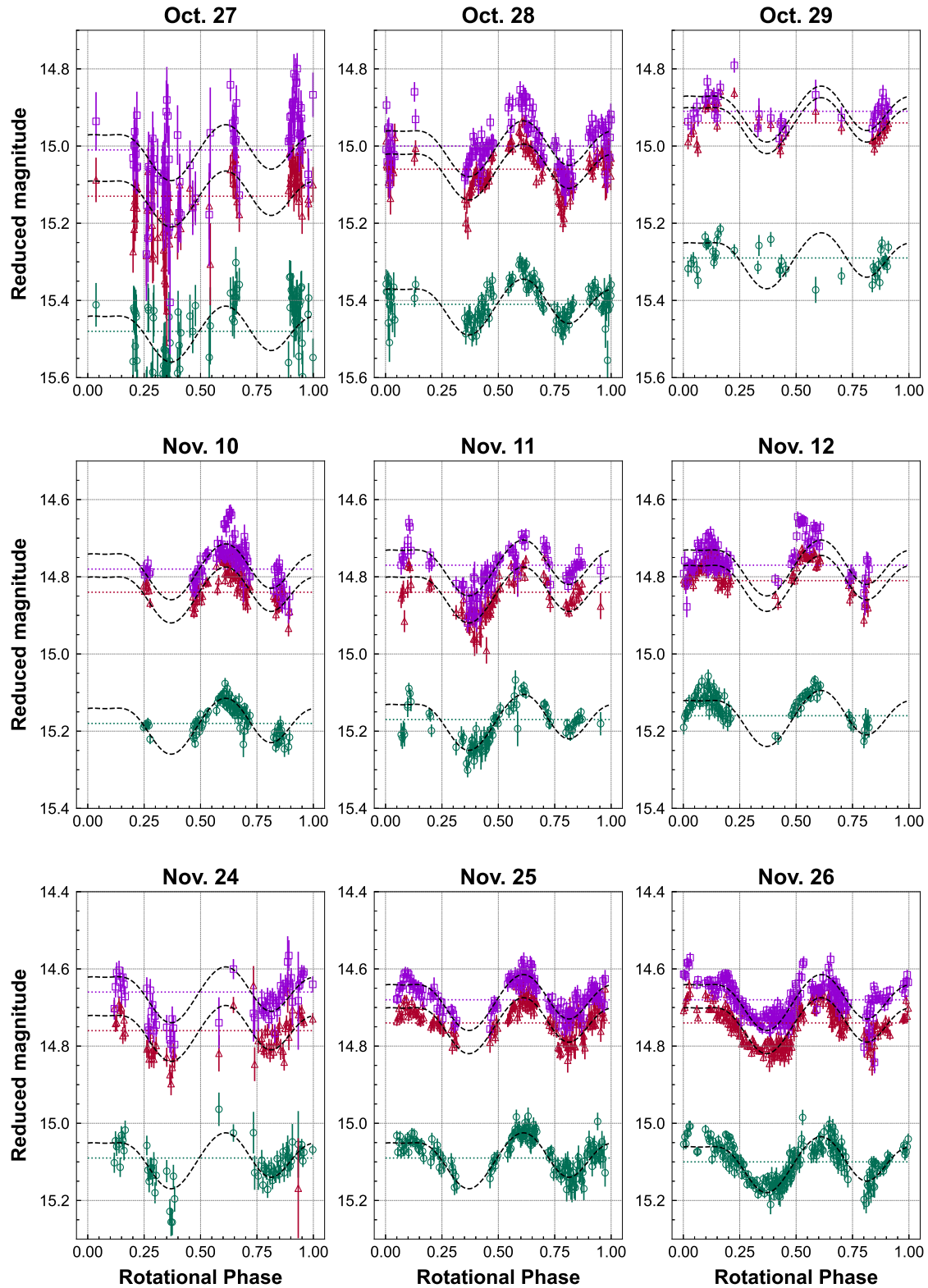


Fig. 7. Phased lightcurves of Phaethon in nine days. From top to bottom, g (circles), r (triangles), and i-band (squares) lightcurves on different days are presented. Bars indicate the $1\text{-}\sigma$ uncertainties. Model curves adopting the number of harmonics $n = 4$ are shown by dashed lines. Mean reduced magnitudes are given as constant terms of the model curves as presented by dotted lines.

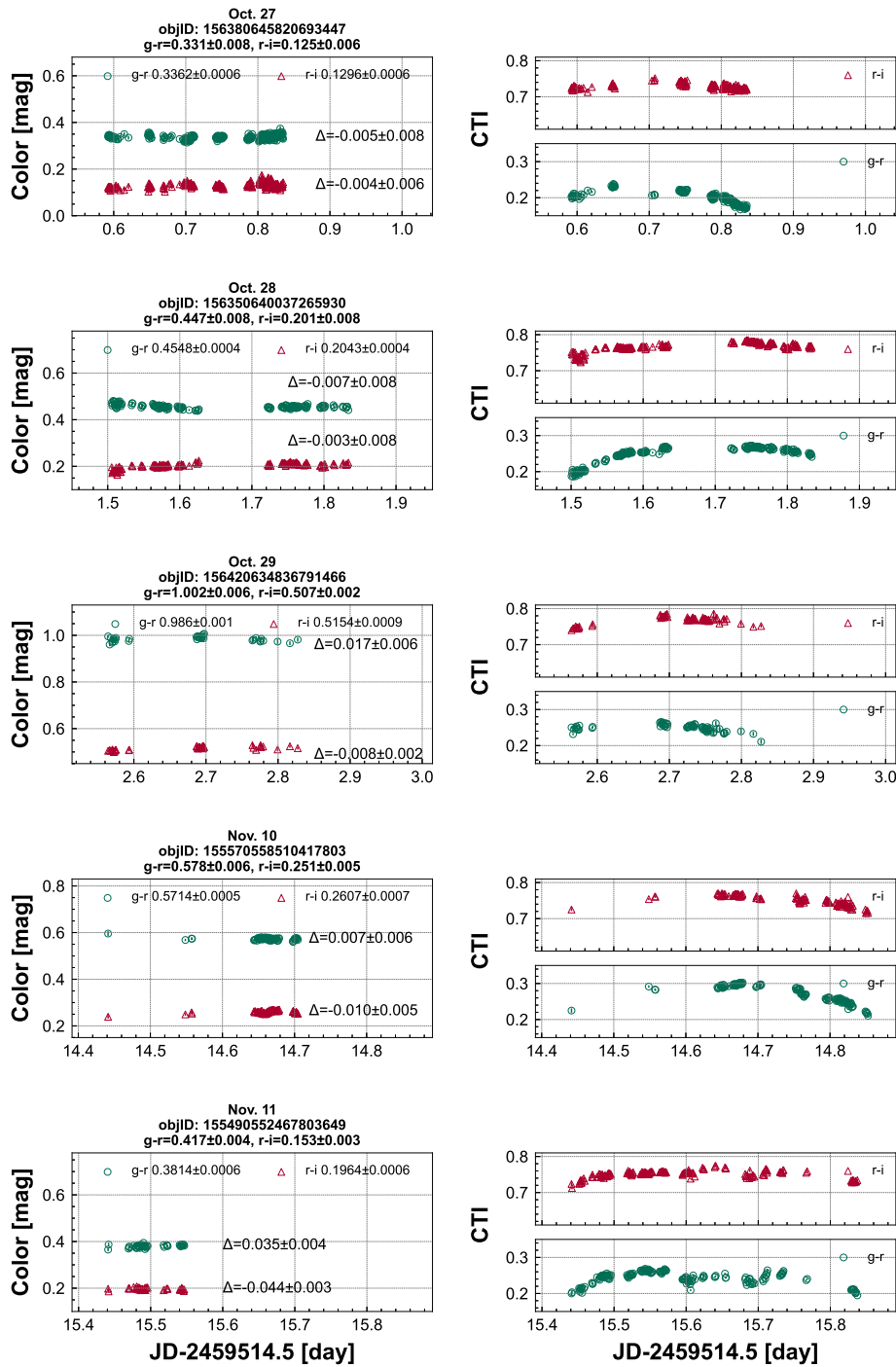


Fig. 8. Colors of reference stars on October 26, 27, 28, November 10, and 11 (left). Object name (objID) and colors in the Pan-STARRS DR2 are written on the top of the panel. $g-r$ and $r-i$ colors are shown by circles and triangles, respectively. Bars indicate the 1- σ uncertainties. The differences Δ , colors in Pan-STARRS DR2 - those derived here, are given. The number of observations of reference stars differs from star to star due to the change of the field of view. Time-series CTIs on October 26, 27, 28, November 10, and 11 (right). CTI_{g-r} and CTI_{r-i} are shown by circles and triangles, respectively. Bars indicate the 1- σ uncertainties.

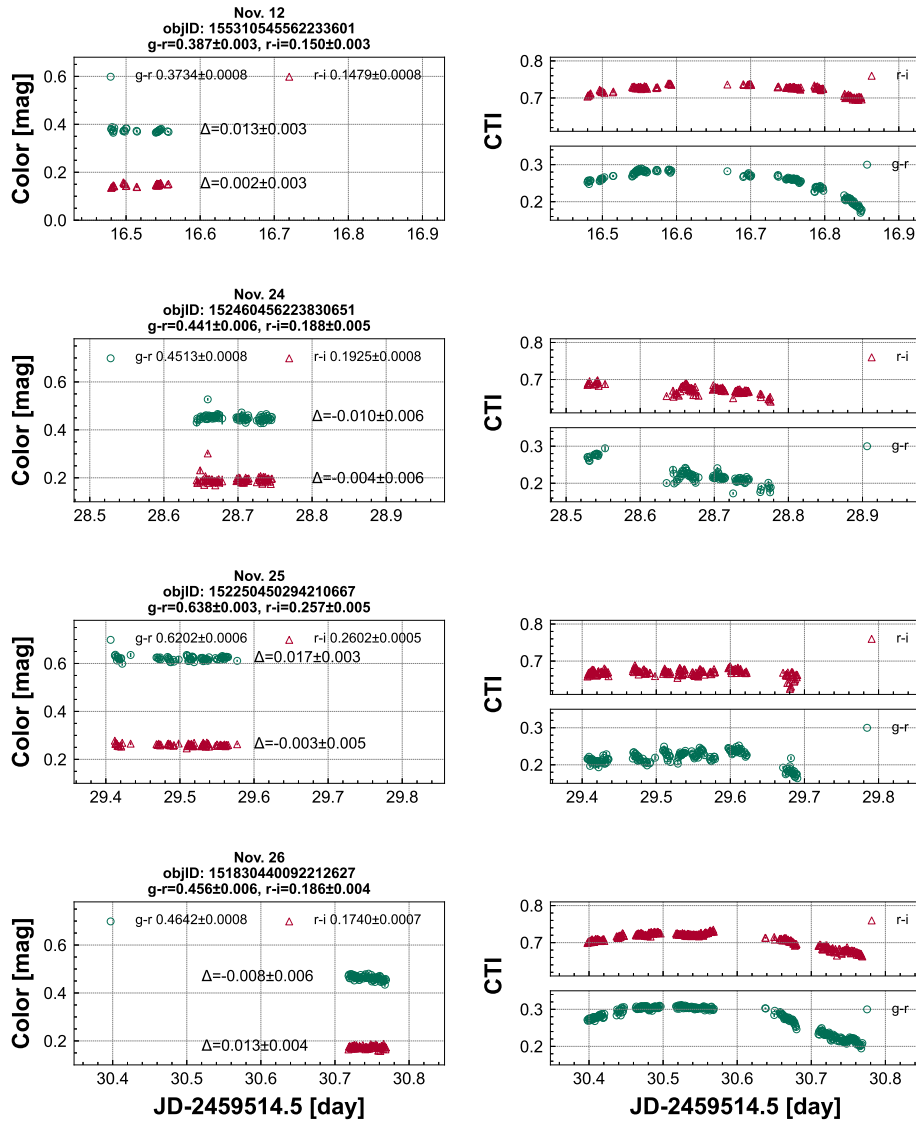


Fig. 9. Same as figure 8 but for November 12, 24, 25, and 26.